



Kent Academic Repository

Maji, Subrata, Gupta, Prachi, Clowes, Rob, Matsushita, Yoshitaka, Shrestha, Lok Kumar, Slater, Anna G., Hill, Jonathan P. and Chahal, Mandeep K. (2026) *Central-metal-cation-based modulation of gas adsorption selectivity in porous tetrapyrrolic materials*. *Chemical Communications* . ISSN 1364-548X.

Downloaded from

<https://kar.kent.ac.uk/113136/> The University of Kent's Academic Repository KAR

The version of record is available from

<https://doi.org/10.1039/d5cc06796k>

This document version

Publisher pdf

DOI for this version

Licence for this version

CC BY-NC (Attribution-NonCommercial)

Additional information

Versions of research works

Versions of Record

If this version is the version of record, it is the same as the published version available on the publisher's web site. Cite as the published version.

Author Accepted Manuscripts

If this document is identified as the Author Accepted Manuscript it is the version after peer review but before type setting, copy editing or publisher branding. Cite as Surname, Initial. (Year) 'Title of article'. To be published in **Title of Journal** , Volume and issue numbers [peer-reviewed accepted version]. Available at: DOI or URL (Accessed: date).

Enquiries

If you have questions about this document contact ResearchSupport@kent.ac.uk. Please include the URL of the record in KAR. If you believe that your, or a third party's rights have been compromised through this document please see our [Take Down policy](https://www.kent.ac.uk/guides/kar-the-kent-academic-repository#policies) (available from <https://www.kent.ac.uk/guides/kar-the-kent-academic-repository#policies>).



Cite this: DOI: 10.1039/d5cc06796k

 Received 29th November 2025,
 Accepted 9th February 2026

DOI: 10.1039/d5cc06796k

rsc.li/chemcomm

Central-metal-cation-based modulation of gas adsorption selectivity in porous tetrapyrrolic materials

 Subrata Maji,^a Prachi Gupta,^{id}^b Rob Clowes,^b Yoshitaka Matsushita,^{id}^c
 Lok Kumar Shrestha,^{id}^a Anna G. Slater,^{id}^b Jonathan P. Hill,^{id}^a and
 Mandeep K. Chahal,^{id}^{*d}

We present a direct strategy to assemble porous tetrapyrrolic materials with tunable gas uptake selectivity by varying the coordinated cation. Co-OX1 shows improved CO₂ uptake of 51.66 cm³ g⁻¹ at 298 K, while free base-OX1 demonstrates a CO₂/N₂ selectivity of 202.9. This approach offers a viable route to CO₂ capture technologies.

A critical driver of climate change is the rising level of atmospheric CO₂, which threatens human health, ecosystems, food security and the global economy.^{1,2} Porous materials are suitable candidates for applications in gas capture technologies.^{3–5} Known porous solids such as zeolites, metal–organic frameworks (MOFs), and covalent organic frameworks (COFs), offer high gas adsorption capacity and selectivity but suffer from poor processability.^{6–8} However, once formed, these porous network materials are difficult to disperse in most media, making deposition on substrates challenging and obstructing applications. As an alternative, porous organic molecular materials such as hydrogen- and halogen-bonded organic frameworks (HOF, XOF, resp.), porous organic cages, supramolecular organic frameworks (SOFs), and π -organic frameworks, lack strong intermolecular bonds between building blocks^{9–12} enabling processing from solution as porous solids or liquids. These porous materials offer various advantages such as ease of structural characterisation, solution processability, tunability, modularity, and ease of regeneration.

Since the emergence of the processable porous materials field, porphyrin-based cages, HOFs, and SOFs have been reported based on intrinsic and/or extrinsic porous networks.^{13–18} Porphyrins are particularly attractive components of porous materials due to their unique tunable photophysical, photochemical, and electrochemical

properties, which allow adaptation to specific functional roles. Topological and pore structure modulation without a requirement for *de novo* design is crucial in porous materials, enabling precise control over molecular diffusion, adsorption selectivity, and host–guest interactions.^{19,20} For porphyrinic HOFs, pore engineering has recently been achieved by introducing structure-directing agents (SDAs) such as solvents,^{16,21} or small cations²² or by varying metal cation coordination.^{23–25}

In general, the metal cation in metalloporphyrins controls the macrocyclic geometry, axial coordination, electronic structure, and intermolecular interactions. Although variation of the coordinated metal cation is known to affect textural properties in metalloporphyrin-based HOFs,^{23–25} there are no reports so far showing that metalation of porphyrins can influence the selectivity of gas adsorption. Despite this, metalation remains a powerful strategy to generate novel porous materials from existing porphyrin building blocks. This raises the intriguing possibility that metalation might be used as a design tool not only to enhance structural stability and engineer pore structure, but also to enable effective access to new processable porous materials with selective gas storage and sensing capabilities.

We have recently reported a nickel-porphyrin-based porous processable framework material that enables highly sensitive

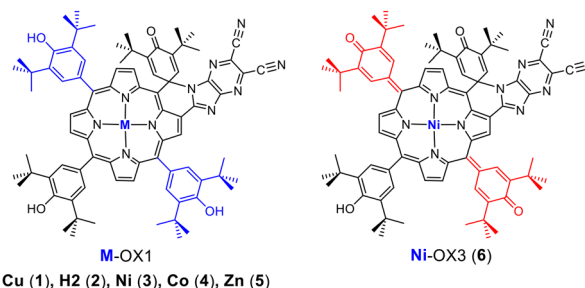


Fig. 1 Chemical structures of M-OX1 and Ni-OX3 compounds synthesised to investigate the effect of metal cations on porous framework structure and gas adsorption selectivity.

^a Research Center for Materials Nanoarchitectonics, National Institute for Materials Science, 1-1 Namiki, Tsukuba, Ibaraki 305-0044, Japan

^b Department of Chemistry and Materials Innovation Factory, University of Liverpool, Liverpool L69 7ZD, UK

^c Research Network and Facility Services Division, National Institute for Materials Science, 1-2-1 Sengen, Tsukuba, Ibaraki 305-0047, Japan

^d Chemistry and Forensic Science, School of Natural Sciences, University of Kent, CT2 7NH Canterbury, UK. E-mail: m.k.chahal@kent.ac.uk



and selective detection of acetone vapour under high humidity conditions.²⁶ Furthermore, analyte specificity can be controlled by varying the molecular structure of the porphyrin.²⁷ This extrinsic porous material is formed through multipoint supra-molecular interactions including π - π stacking, metal coordination, and hydrogen bonding.

To build on this, we hypothesised that variation of metalation could influence supramolecular interactions and crystal packing due to conformational and coordinative changes at the porphyrin core, which might lead to gas uptake selectivities. Here, we report a series of metalloporphyrin compounds, Cu-OX1 (1), H2-OX1 (2), Ni-OX1 (3), Co-OX1 (4), Zn-OX1 (5) and Ni-OX3 (6), where the effect of the central metal atom (or its absence) on the porosity of the resulting processable porous materials (Fig. 1) and also the potential of these materials for selective CO₂/N₂ uptake, have been studied. Synthetic details are given in the SI. Co-OX1 (4) was synthesised by exchanging Ni(II) for Co(II) since the formylation route previously used for Ni-OX1 (3)²⁸ is incompatible with Co(II), leading to mixtures of oxidised products. Cu-OX1 (1) was synthesised following the formylation route, followed by reaction with 5,6-diaminopyrazine-2,3-dicarbonitrile, then oxidation using DDQ or PbO₂. The compounds were characterised using spectroscopic techniques (Fig. S1–S9) and single crystal X-ray diffraction studies.

Single crystals of Cu-OX1 (1), Ni-OX1 (3), Co-OX1 (4) and Ni-OX3 (6) were grown from suitable solvents. Ni-OX1 (3) (CCDC number: 1920462)²⁹ and Ni-OX3 (6) (CCDC numbers: 2107801–2107804)²⁶ were reported previously.²⁶ The complexes exhibit supramolecular structures formed through different non-covalent interactions (π - π stacking, hydrogen bonding, metal to ligand co-ordination); see Fig. S10–S27. For Cu-OX1 (1), there are four molecules per unit cell with π - π bonds (dimer shortest distance of 3.38(1) Å) and an H-bond, 3.49(8) Å between C=O and phenol H. CHCl₃ molecules are trapped inside the extended framework as shown in Fig. S11. Molecules of Ni-OX1 (3) form π - π dimers in the solid state with a short intermolecular closest approach of 3.28(4) Å and a C≡N...Ni(II) distance of 3.52(9) Å (Fig. S17). Co-OX1 (4) forms an extended network similar to Cu-OX1 (1) with a π -stacking distance of 3.30(9) Å and a longer H-bond distance of 3.55(6) Å between C=O and phenol H (Fig. S22). The magnitude of mean displacement of the 24-atom core ($\Delta 24$) and β -pyrrole carbons in Ni-OX1 (3) ($\Delta 24 = 0.284$ Å, $\Delta C_{\beta} = 0.365$ Å) and Ni-OX3 (6) ($\Delta 24 = 0.471$ Å, $\Delta C_{\beta} = 0.330$ Å) is much larger than in Cu-OX1 (1) ($\Delta 24 = 0.070$ Å, $\Delta C_{\beta} = 0.072$ Å) or Co-OX1 (4) ($\Delta 24 = 0.090$ Å, $\Delta C_{\beta} = 0.135$ Å) suggesting that both Cu-OX1 (1) and Co-OX1 (4) have quasi-planar conformations while the Ni-complexes in both OX1 and OX3 forms are nonplanar (Fig. S28).

The crystalline nature of the compounds was confirmed by powder X-ray diffraction (PXRD) studies (Fig. S29), and their permanent porosities were investigated by measuring N₂ sorption isotherms at 77 K (Fig. 2). To ensure removal of guest molecules, all samples were degassed under vacuum at 120 °C for 24 h prior to N₂ sorption measurements. Important textural parameters derived from these measurements are shown in Table S1, indicating that each system exhibits characteristic N₂ uptake, Brunauer–Emmett–Teller (BET) surface area and pore

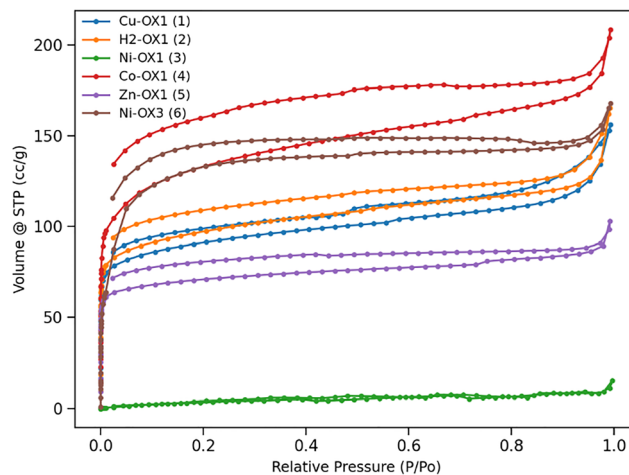


Fig. 2 N₂ adsorption–desorption isotherms at 77 K for M-OX1 and Ni-OX3 materials.

volume. Ni-OX1 (3) shows negligible N₂ uptake (15.33 cm³ g⁻¹) with a BET surface area of 15.12 m² g⁻¹. Previously, we proposed that a highly non-planar porphyrin core ($\Delta 24$ displacement of the porphyrin mean planes) was required for effective N₂ adsorption.²⁶ However, surprisingly, the planar derivatives Cu-OX1 (1) and Co-OX1 (4) exhibit some of the largest BET surface areas and N₂ uptakes. This observation suggests that the porphyrin core structure is not the only factor influencing adsorption properties in these systems, but metalation and/or the identity of the coordinated metal atom also plays a significant role in influencing gas adsorption. The BET surface areas, N₂ uptakes and corresponding pore volumes for each system are summarised in Table 1.

Given the different N₂ uptakes at 77 K under gas saturation conditions, we proceeded to investigate CO₂ uptake at 195 K and also under saturation conditions to assess the maximum CO₂ adsorption capacity of these complexes (Fig. 3). The CO₂ uptake capacities shown in Table 1 indicate that Ni-OX3 (6) has the lowest affinity towards CO₂. CO₂ and N₂ uptake data at 195 K and 77 K, respectively, reveal that Ni-OX1 (3) exhibits a substantially higher affinity for CO₂ (106.65 cm³ g⁻¹) than for N₂ (15.33 cm³ g⁻¹). This suggests an ultra-microporous structure since enhanced CO₂ uptake is most likely due to the smaller kinetic diameter of CO₂, which facilitates its diffusion into smaller pores. This observation is consistent with Ni-OX1 (3) having the lowest pore volume (0.040 cm³ g⁻¹) of the systems studied. All the materials studied show significant CO₂ uptakes

Table 1 BET surface areas (in m² g⁻¹), N₂ uptakes and corresponding pore volumes (cm³ g⁻¹) at 77 K, and CO₂ uptakes (in cm³ g⁻¹) at 195 K for M-OX1 and Ni-OX3 complexes

Compound	BET surface areas	N ₂ uptakes	Pore volumes	CO ₂ uptakes
Cu-OX1 (1)	450.57	156.14	0.304	127.96
H2-OX1 (2)	450.71	165.28	0.296	133.94
Ni-OX1 (3)	15.12	15.33	0.040	106.65
Co-OX1 (4)	509.91	208.51	0.338	120.41
Zn-OX1 (5)	346.58	103.10	0.162	122.15
Ni-OX3 (6)	343.56	167.95	0.249	95.07



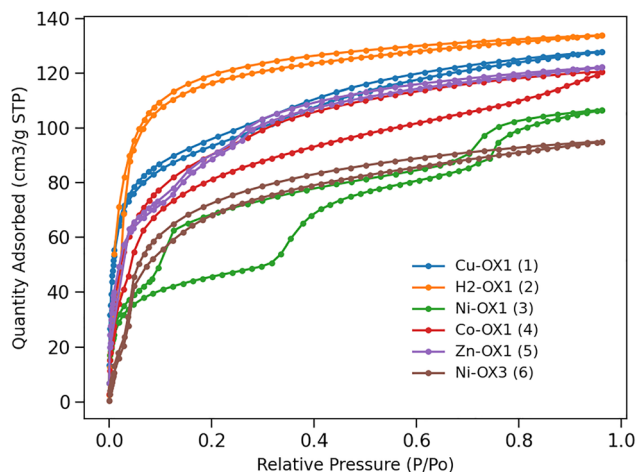


Fig. 3 CO₂ adsorption-desorption isotherms at 195 K for M-OX1 and Ni-OX3 materials.

making them suitable for applications involving efficient CO₂ adsorption, such as gas separation or carbon capture. Both Ni-OX1 (3) and Co-OX1 (4) exhibit hysteresis in their adsorption/desorption curves which can be attributed to phase transition occurring during the process. These phenomena are also confirmed by the PXRD patterns obtained before and after CO₂ adsorption as shown in Fig. S32 and S33 where the PXRD patterns differ especially in the low angle regions.

PXRD data obtained prior to and following CO₂ uptake studies indicate that the crystalline structure is retained after

activation at 110 °C, although some phase transitions in the materials are observed (Fig. S30–35). Thermogravimetric analyses (Fig. S36) of the porous frameworks indicate weight losses starting at 50 °C complete by 170 °C assigned to solvent losses. The materials then exhibit a steady plateau up to 380 °C, followed by weight losses of 45–59% occurring up to 900 °C assigned to decomposition. These data indicate that both the free-base and metal complexes have excellent thermal stability.

Considering the excellent thermal stability and selective gas uptake by Ni-OX1 (3), the suitability of these porphyrin complexes for gas separation applications was studied. While processable porous materials have been studied for gas separation, the impact of metalation and central atom identity at the porphyrin core remains unexplored, although it might be used to identify a wide range of useful materials without the need for *de novo* design. For this purpose, we conducted N₂ and CO₂ sorption experiments both at 273 K and 298 K (Fig. 4). All the materials studied show higher CO₂ uptakes at both 273 K and 298 K than their N₂ adsorption capacities as shown in Table 2. H2-OX1 (2) demonstrated the highest CO₂ uptake of 67.65 cm³ g⁻¹ at 273 K when compared to metal-containing compounds. However, at 298 K, the CO₂ uptake of the metal compounds exceeded that of H2-OX1 (2), with Co-OX1 (4) showing the highest uptake of 51.66 cm³ g⁻¹. These uptake values at 298 K are important for practical applications, as direct CO₂ capture from the atmosphere under ambient conditions is the key for industrial processes. These results highlight the role of metal ions in tuning the CO₂ uptake behaviour. Additionally, these CO₂ adsorption capacities are larger than

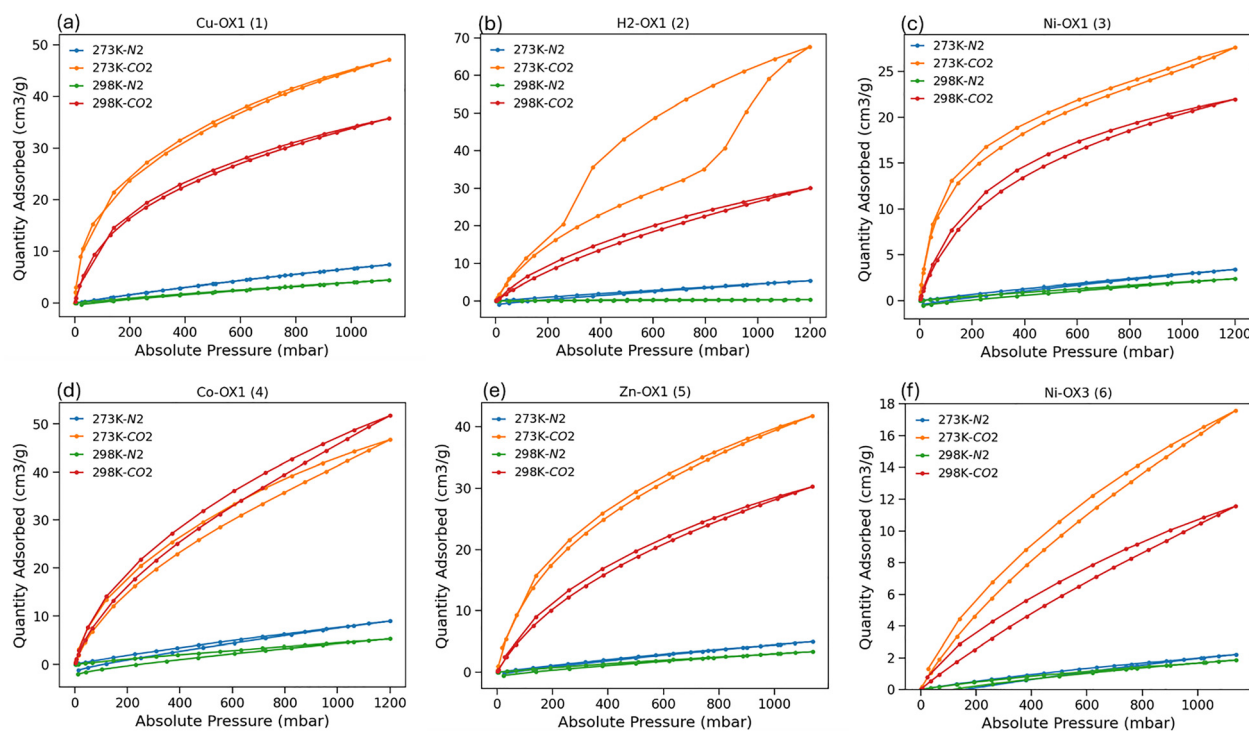


Fig. 4 CO₂ and N₂ adsorption isotherms at 273 K and 298 K, respectively for (a) Cu-OX1 (1); (b) H2-OX1 (2); (c) Ni-OX1 (3); (d) Co-OX1 (4); (e) Zn-OX1 (5); and (f) Ni-OX3 (6).



Table 2 CO₂ and N₂ adsorption capacities (in cm³ g⁻¹) at 273 K and 298 K for M-OX1 and Ni-OX3 complexes

Compound	CO ₂ uptakes at 273 K	CO ₂ uptakes at 298 K	N ₂ uptakes at 273 K	N ₂ uptakes at 298 K
Cu-OX1 (1)	47.06	35.76	7.39	4.41
H2-OX1 (2)	67.65	30.04	5.36	0.38
Ni-OX1 (3)	27.61	21.96	3.39	2.37
Co-OX1 (4)	46.67	51.66	8.95	5.27
Zn-OX1 (5)	41.79	30.28	4.99	3.37
Ni-OX3 (6)	17.59	11.57	2.21	1.86

those already reported for other processable porphyrinic porous organic molecular materials (see Table S2) making our materials a significant advance in terms of possible applications. In this study, CO₂ sorption measurements were performed on the same samples at three different temperatures (195 K, 273 K, and 298 K), which indicates that the samples exhibit porosity over multiple measurement cycles. The N₂ adsorption capacities of these materials are significantly lower, ranging from 0.38 to 8.95 cm³ g⁻¹, highlighting their selectivity of adsorption. Also, Ni-OX3 (6) exhibits the lowest CO₂ sorption. The significant differences in CO₂ and N₂ adsorption capacities suggest that these materials could be effective for CO₂/N₂ separation. CO₂/N₂ selectivity was determined using the ideal adsorbed solution theory (IAST),^{30,31} a reliable method for predicting selectivity in binary gas separations (Fig. S37–S48). For a 0.15/0.85 CO₂/N₂ mixture, the highest selectivity of 143.4 was calculated for H2-OX1 (2) at 298 K and 0.1 bar, but metal complexes also demonstrate good selectivity. For example, Cu-OX1 (1) has a selectivity of 44.0 and Ni-OX1 (3) showed a value of 34.8 at 0.1 bar. At 273 K, the IAST selectivity differs: Cu-OX1 (1) shows the highest CO₂/N₂ selectivity of 77.8 at 0.1 bar, followed by Ni-OX1 (3) with a selectivity of 72.7. In contrast, H2-OX1 (2) has a significantly lower selectivity of 9.2 at 0.1 bar. These high selectivity values indicate that varying the central atom in porphyrinic systems can be used to tune the properties of materials for gas separation applications.

In conclusion, we report the modulation of the CO₂/N₂ gas adsorption capabilities of a family of supramolecular porous porphyrins by varying the coordinated metal cation. Under saturation conditions, Ni-OX1 (3) shows negligible N₂ uptake (15.33 cm³ g⁻¹) while Ni-OX3 (6) and other metal and free-base OX1 complexes show significant adsorption. OX1 systems show substantial CO₂ uptake (up to 133.94 cm³ g⁻¹ for H2-OX1) at 195 K. Further experiments at 278 K and 298 K, along with IAST calculations, confirm selective CO₂ adsorption and separation. These materials are solution processable, and their solubility in common organic solvents offers an additional advantage by enabling applications beyond bulk sorption experiments, such as thin-film fabrication and device integration.

SM, PG, RC, YM, and LKS: investigation; validation; writing – review and editing. AGS, JPH: supervision; validation; writing – review and editing; funding acquisition. MKC: conceptualization; funding acquisition; synthesis; writing – original draft, review and editing.

MKC thanks the Royal Society of Chemistry (R23-0850952021) and the Royal Society (RG\R1\251071) for funding. AGS thanks the

Royal Society for a University Research Fellowship (URF\R1\201168). This work made use of shared equipment at the Materials Innovation Factory (MIF) created as part of the UK Research Partnership Innovation Fund (Research England) and co-funded by the Sir Henry Royce Institute.

Conflicts of interest

There are no conflicts to declare.

Data availability

The data supporting this article have been included in the supplementary information (SI). Supplementary information: experimental methods, crystallographic details, thermal analysis, PXRD patterns, and IAST plots for selectivity prediction. See DOI: <https://doi.org/10.1039/d5cc06796k>.

CCDC 2501550 and 2501551 contain the supplementary crystallographic data for this paper.^{32a,b}

References

- 1 D. Wang, J. Penuelas, Y. Tao, I. Loladze, C. Cai, L. Song, J. Zhang, G. Zhang, Y. Wang, W. Zhou, Q. Li and C. Zhu, *Global Change Biol.*, 2025, **31**, e70299.
- 2 L. J. R. Nunes, *Environments*, 2023, **10**, 66.
- 3 L. Pan, K. M. Adams, H. E. Hernandez, X. Wang, C. Zheng, Y. Hattori and K. Kaneko, *J. Am. Chem. Soc.*, 2003, **125**, 3062–3067.
- 4 L. Wang and R. Yang, *J. Phys. Chem. C*, 2011, **115**, 21264–21272.
- 5 A. H. Farmahini, S. Krishnamurthy, D. Friedrich, S. Brandani and L. Sarkisov, *Chem. Rev.*, 2021, **121**, 10666–10741.
- 6 N. Stock and S. Biswas, *Chem. Rev.*, 2012, **112**, 933–969.
- 7 G. Zhang, B. Hua, A. Dey, M. Ghosh, B. A. Moosa and N. M. Khashab, *Acc. Chem. Res.*, 2021, **54**, 155–168.
- 8 A. G. Slater and A. I. Cooper, *Science*, 2015, **348**, aaa8075.
- 9 J. Tian, P. K. Thallapally and B. P. McGrail, *CrystEngComm*, 2012, **14**, 1909–1919.
- 10 P. Sun, H. Dong, S. Lv, Y. Yin, G. Gong, L. Wang, J. Wang and S. Chen, *J. Mater. Chem. A*, 2024, **12**, 1128–1134.
- 11 Z. J. Lin, S. A. R. Mohammed, T. F. Liu and R. Cao, *ACS Cent. Sci.*, 2022, **8**, 1589–1608.
- 12 M. Liu, M. A. Little, K. E. Jelfs, J. T. A. Jones, M. Schmidtman, S. Y. Chong, T. Hasell and A. I. Cooper, *J. Am. Chem. Soc.*, 2014, **136**, 7583–7586.
- 13 S. Hong, Md. R. Rohman, J. Jia, Y. Kim, D. Moon, Y. Kim, Y. H. Ko, E. Lee and K. Kim, *Angew. Chem., Int. Ed.*, 2015, **127**, 13439–13442.
- 14 W. Yang, B. Li, H. Wang, O. Alduhaish, K. Alfooty, M. A. Zayed, P. Li, H. D. Arman and B. Chen, *Cryst. Growth Des.*, 2015, **15**, 2000–2004.
- 15 Y. N. Gong, D. C. Zhong and T. B. Lu, *Angew. Chem., Int. Ed.*, 2025, **64**, e202424452.
- 16 L. Ma, H. Arman, Y. Xie, W. Zhou and B. Chen, *Cryst. Growth Des.*, 2022, **22**, 3808–3814.
- 17 J. H. Lee, H. Park, Y. Kim, D. Yim, T. Kim, J. Choi, Y. Lee and W. D. Jang, *ACS Appl. Mater. Interfaces*, 2023, **15**, 57507–57513.
- 18 W. Yang, F. Yang, T. L. Hu, S. C. King, H. Wang, H. Wu, W. Zhou, J. R. Li, H. D. Arman and B. Chen, *Cryst. Growth Des.*, 2016, **16**, 5831–5835.
- 19 A. G. Slater, P. S. Reiss, A. Pulido, M. A. Little, D. L. Holden, L. Chen, S. Y. Chong, B. M. Alston, R. Clowes, M. Haranczyk, M. E. Briggs, T. Hasell, G. M. Day and A. I. Cooper, *ACS Cent. Sci.*, 2017, **3**, 734–742.
- 20 M. O'Shaughnessy, P. R. Spackman, M. A. Little, L. Catalano, A. James, G. M. Day and A. I. Cooper, *Chem. Commun.*, 2022, **58**, 13254–13257.
- 21 X. T. He, Y. H. Luo, Z. Y. Zheng, C. Wang, J. Y. Wang, D. L. Hong, L. H. Zhai, L. H. Guo and B. W. Sun, *ACS Appl. Nano Mater.*, 2019, **2**, 7719–7727.
- 22 Y. Cai, J. Gao, J. H. Li, P. Liu, Y. Zheng, W. Zhou, H. Wu, L. Li, R. B. Lin and B. Chen, *Angew. Chem., Int. Ed.*, 2023, **62**, e202308579.



- 23 P. Tholen, C. A. Peeples, M. M. Ayhan, L. Wagner, H. Thomas, P. Imbrasas, Y. Zorlu, C. Baretzky, S. Reineke, G. Hanna and G. Yücesan, *Small*, 2022, **18**, 2204578.
- 24 Q. Yin, E. V. Alexandrov, D. H. Si, Q. Q. Huang, Z. Bin Fang, Y. Zhang, A. A. Zhang, W. K. Qin, Y. L. Li, T. F. Liu and D. M. Proserpio, *Angew. Chem., Int. Ed.*, 2022, **61**, e202115854.
- 25 S. Huang, Y. Chang, Z. Li, J. Cao, Y. Song, J. Gao, L. Sun and J. Hou, *Adv. Funct. Mater.*, 2023, **33**, 2211631.
- 26 M. K. Chahal, S. Maji, A. Liyanage, Y. Matsushita, P. Tozman, D. T. Payne, W. Jevasuwan, N. Fukata, P. A. Karr, J. Labuta, L. K. Shrestha, S. Ishihara, K. Ariga, F. D'Souza, G. Yoshikawa, Y. Yamauchi and J. P. Hill, *Mater. Chem. Front.*, 2023, **7**, 325–332.
- 27 S. Maji, J. Hynek, K. Nakada, A. Hori, K. Minami, J. Labuta, M. K. Chahal, D. T. Payne, G. J. Richards, L. K. Shrestha, K. Ariga, Y. Yamauchi, G. Yoshikawa and J. P. Hill, *Adv. Mater. Technol.*, 2025, **10**, e00294.
- 28 M. K. Chahal and M. Sankar, *Dalton Trans.*, 2016, **45**, 16404–16412.
- 29 M. K. Chahal, J. Labuta, V. Březina, P. A. Karr, Y. Matsushita, W. A. Webre, D. T. Payne, K. Ariga, F. D'Souza and J. P. Hill, *Dalton Trans.*, 2019, **48**, 15583–15596.
- 30 C. M. Simon, B. Smit and M. Haranczyk, *Comput. Phys. Commun.*, 2016, **200**, 364–380.
- 31 Mantid, *Manipulation and Analysis Toolkit for Instrument Data*, 2013, Mantid Project, DOI: [10.5286/SOFTWARE/MANTID6.14](https://doi.org/10.5286/SOFTWARE/MANTID6.14).
- 32 (a) CCDC 2501550: Experimental Crystal Structure Determination, 2026, DOI: [10.5517/ccdc.csd.cc2pz25y](https://doi.org/10.5517/ccdc.csd.cc2pz25y); (b) CCDC 2501551: Experimental Crystal Structure Determination, 2026, DOI: [10.5517/ccdc.csd.cc2pz26z](https://doi.org/10.5517/ccdc.csd.cc2pz26z).

